Hyperfine structure in the $4p^5 5d$ states of ^{83}Kr

Rupesh Silwal and J. R. Brandenberger

Department of Physics, Lawrence University, Appleton, Wisconsin 54912, USA

(Received 9 January 2006; published 15 March 2006)

Hyperfine splittings in the $4d_1'$, $4d_3$, $4d_4$, and $4d_5$ states of the $4p^5 5d$ configuration of ^{83}Kr ($I=9/2$) have been measured using two-step laser excitation. The corresponding hyperfine coupling constants A and B are negative (with one exception) and range from -400 to $+85$ MHz.

PACS number(s): 32.10.Fn, 32.30.−r, 32.70.Jz

I. INTRODUCTION

Numerous measurements of fine and hyperfine splittings in the low-lying $4p^5 5s$ and $4p^5 5p$ manifolds of ^{83}Kr have advanced our understanding of the structural subtleties of the ^{83}Kr atom and shed light on broader issues such as relativistic, electron-correlation, core-polarization and configuration-mixing contributions to the fine and hyperfine structure in rare-gas atoms [1–3]. While a few measurements of hyperfine structure (hfs) in states lying above the $4p^5 5s$ and $4p^5 5p$ manifolds have been reported, to date there has been no systematic effort to measure and compare the hfs in the closely related and close-lying fine-structure states that make up the $4p^5 5d$ or higher-lying configurations of ^{83}Kr. To reverse this situation, we have undertaken a systematic investigation of the hfs in the $4p^5 5d$ manifold of ^{83}Kr using a two-step, sub-Doppler type of laser spectroscopy. This paper reports measurements of hyperfine splittings in four fine-structure levels of the $4p^5 5d$ configuration of ^{83}Kr and compares the ordering and interval spacings of the various hyperfine levels.

II. EXPERIMENTAL ARRANGEMENT

The experimental layout for our version of two-step laser spectroscopy appears in Fig. 1. The main target cell shown at the lower left is cylindrical in shape, 150 mm in length by 18 mm in diameter, and filled with approximately 200 mTorr of krypton gas isotopically enriched to 73% ^{83}Kr, 22% ^{82}Kr, and 5% ^{84}Kr [4]. To populate the low-lying $4p^5 5s$ states of ^{83}Kr, which serve as pseudoground states in this work, we use a 30-MHz oscillator [5] to excite an rf discharge in the target cell via external electrodes that produce rf fields of about 20 V/cm. The discharge is sufficiently weak to leave the cell near room temperature even though the electron temperature is $5-10$ eV. The number density of the krypton target is 6×10^{15} atoms/cm^3; we estimate the $1s_5$ population in the $4p^5 5s$ configuration to be 10^{13} atoms/cm^3 but presume the $4p^5 5p$ and $4p^5 5d$ populations to be considerably smaller [6].

The various two-step excitation schemes employed in this work are shown in Fig. 2. Laser 1, whose wavelength is 892.869, 810.436, or 760.154 nm, promotes metastable $4p^5 5s$ ^{83}Kr atoms lying in the $1s_5$ level into the $2p_{10}$, $2p_8$, or $2p_6$ fine-structure state in the $4p^5 5p$ manifold [7]. All of our first-step excitations originate in the $1s_5$ level of the $4p^5 5s$ manifold since it contains a sizeable population generated by the rf excitation.

The experimental layout includes a saturation spectrometer used to identify the desired first-step hfs transition to be pumped by laser 1. Once the desired transition is identified, the scanning of laser 1 is reduced to zero, and the frequency of this laser is fixed on this particular line (which is always one of the strongest hfs transitions in the particular $1s_5$ $-2p_j$ cluster). It follows that laser 1 performs both state and velocity selection on a narrow $v \approx 0$ velocity group within the $1s_5$ population [8]. Laser 2 then further promotes these $v \approx 0$ ^{83}Kr atoms into the desired hfs final states of the $4p^5 5d$ configuration. Wavelengths of 827.236 or 841.243 nm lift ^{83}Kr from the $2p_6$ to $4d_1'$ or $4d_3$ states, 792.860 nm excites ^{83}Kr atoms from the $2p_8$ to $4d_4$, and 791.342- and 774.345-nm laser light excites $2p_{10}$ Kr atoms to the $4d_5$ and $4d_6$ states, respectively.

An auxiliary beam emitted by laser 2 passes through a fixed Fabry-Perot cavity. This cavity consists of a 90% reflecting planoconcave mirror with radius of curvature of 1.0 m placed at a distance of 1.0 m from a 90% reflecting planar mirror. This arrangement creates an optical cavity whose effective length is 4.0 m and whose free spectral range is about 37.50 MHz. The comb of interference fringes produced by this interferometer is used to determine the frequency separations in the spectra generated by the second-
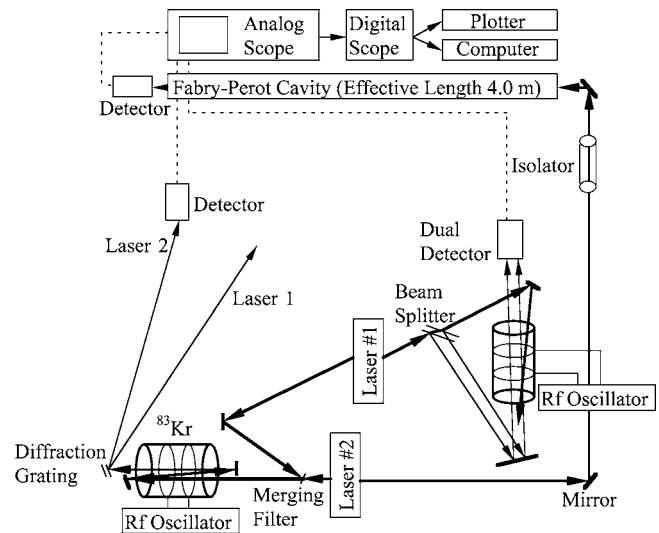
FIG. 1. Experimental layout for two-step, sub-Doppler laser spectroscopy. The lasers are scanned with a ramp derived from the analog oscilloscope.
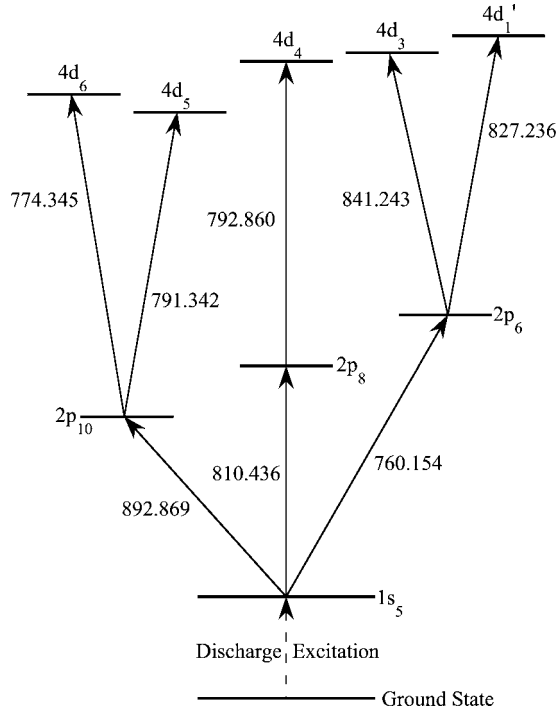
FIG. 2. Two-step excitation schemes for accessing various hfs states in the $4p^55d$ manifold of ^{83}Kr. The $4d_6(J=0)$ state contains no hfs. All wavelengths are in nm.

step of laser excitation. In performing this measurement, we use only that part of the interferogram that corresponds precisely to the separation between the spectral peaks. The use of only this part of the interferogram mitigates the effects of frequency nonuniformities or nonlinearities in the scanning of laser 2 [9]. A diffraction grating separates the two laser beams emerging from the sample cell; we record only the absorption spectra riding on the beam from laser 2.

All lasers are custom-designed, external-cavity, single-mode diode lasers that employ commercially available laser diodes [10]. The output powers of these Littrow-configured lasers range from 5–20 mW, and their spectral widths are about 1 MHz. The laser beam intensities in the sample cell are approximately 2 mW/mm^2.

Real-time monitoring of the absorption spectra on the oscilloscope, whose ramp sweeps the lasers, facilitates optimization of the experiment. The raw 10-mV spectra 100 msec in length exhibit signal-to-noise (S/N) ratios of about 5. For S/N enhancement and signal capture, these spectra are averaged by a digital oscilloscope that offers a high sampling rate and ten-bit vertical resolution. By averaging 256 successive sweeps, we enhance the S/N ratio to 30 or thereabouts and capture the spectra in digital format. The resulting line shapes consisting of 500 points are dumped to a plotter or computer for processing.

III. THEORY

Hyperfine structure stems from the interaction of nuclear moments with fields produced by the electrons. Parity and time-reversal symmetry dictate that the only nonzero 2^k-pole

moments have odd k for magnetic moments and even k for electric moments. For non-s-electrons, the magnetic dipole and electric quadrupole interactions are similar in magnitude and vastly larger than all higher-order interactions [11].

Since we treat J and I as good quantum numbers, the magnetic dipole Hamiltonian is

$$H = - \boldsymbol{\mu}_I \cdot \boldsymbol{B}_{el}, \qquad (1)$$

where $\boldsymbol{\mu}_I$ is the nuclear magnetic moment and $\boldsymbol{B}_{el}$ is the magnetic field produced at the nucleus by the electrons. Since $\boldsymbol{\mu}_I$ is proportional to $\boldsymbol{I}$ and $\boldsymbol{B}_{el}$ to $\boldsymbol{J}$, this Hamiltonian becomes

$$H = A(J)\boldsymbol{I} \cdot \boldsymbol{J}. \qquad (2)$$

To first order, the shift of a level J due to this interaction is

$$\Delta E = \frac{1}{2}A(J)\{F(F+1) - J(J+1) - I(I+1)\}, \qquad (3)$$

where F is the total angular momentum. The coupling constant $A(J)$ provides a measure of the splitting between various F levels and appears in the *interval rule*

$$\Delta E(F) - \Delta E(F-1) = A(J)F, \qquad (4)$$

where a positive $A(J)$ indicates normal hfs ordering whereas a negative $A(J)$ implies inverted hfs.

The Hamiltonian for the electric quadrupole interaction is

$$H_Q = eQ\left\langle \frac{\partial^2 V_e}{\partial z^2} \right\rangle \frac{\left[3(\boldsymbol{I} \cdot \boldsymbol{J})^2 + \frac{3}{2}\boldsymbol{I} \cdot \boldsymbol{J} - I(I+1)J(J+1) \right]}{2I(2I-1)J(2J-1)}, \qquad (5)$$

where Q is the nuclear quadrupole moment and $\langle \partial^2 V_e/\partial z^2 \rangle$ is the electric-field gradient produced by the electrons at the nucleus. The factor $\langle \partial^2 V_e/\partial z^2 \rangle$ is proportional to $\langle 1/r_e^3 \rangle$, where r_e is the distance between the electron and nucleus [11]. To first order, the quadrupole interaction shifts the energies in accordance with

$$\Delta E = \frac{B}{4}\frac{\frac{3}{2}C(C+1) - 2I(I+1)J(J+1)}{I(2I-1)J(2J-1)}, \qquad (6)$$

where $C \equiv F(F+1) - J(J+1) - I(I+1)$ and $B = eQ\langle \partial^2 V_e/\partial z^2 \rangle$ is the electric quadrupole coupling constant. Combining these two interactions, one finds that the frequency of each hfs sublevel associated with a given fine-structure level is

$$\nu_F = \nu_0 + A\frac{C}{2} + B\frac{\frac{3}{4}C(C+1) - I(I+1)J(J+1)}{2I(2I-1)J(2J-1)}, \qquad (7)$$

where ν_0 is the frequency of the unperturbed fine-structure level. By subtracting Eq. (7) from itself for two different values of F, one can derive expressions for the splittings between pairs of hyperfine levels in terms of A and B. Two such expressions along with two measured splittings are then used to determine A and B.
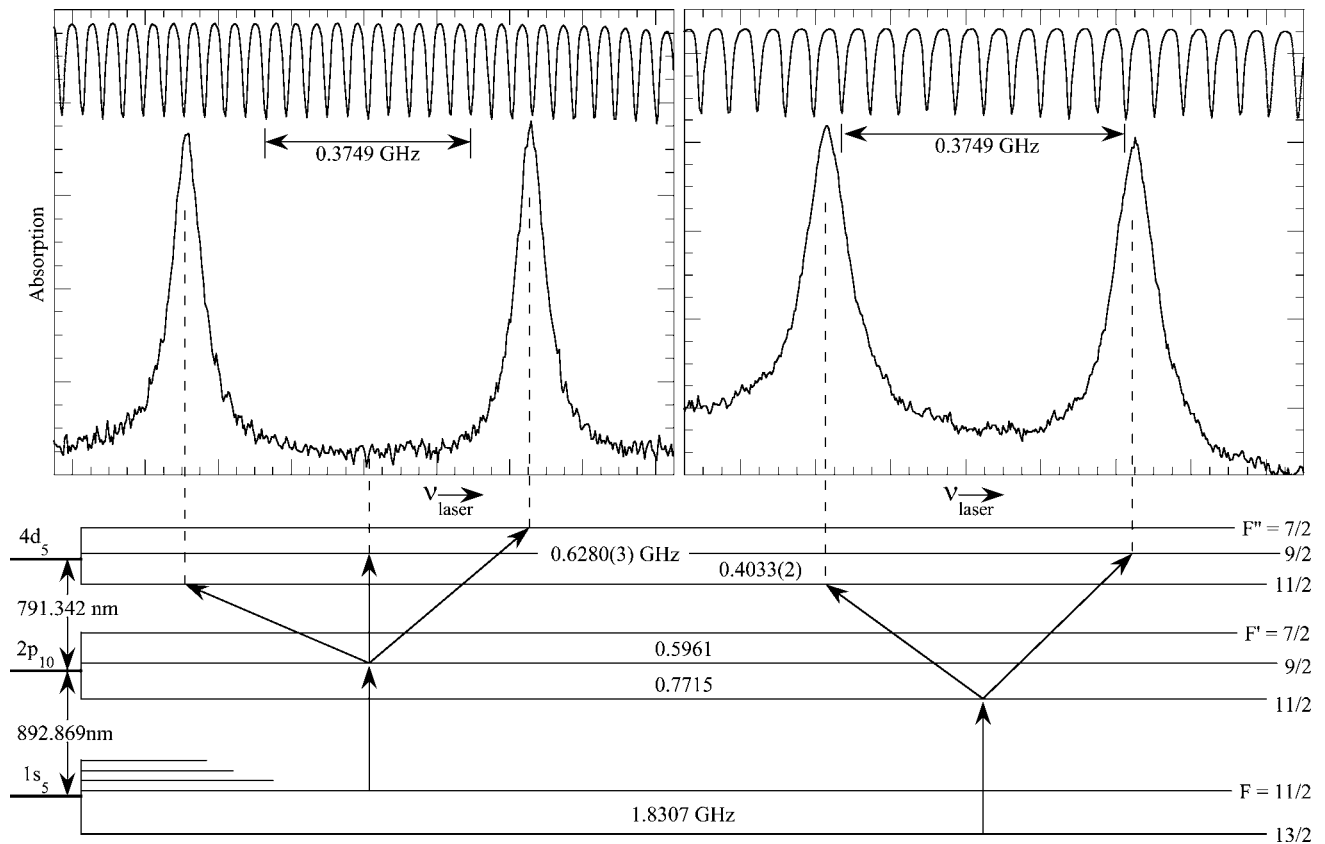
FIG. 3. Two-step spectra and excitation schemes for measuring hfs splittings in the $4d_5$ state of ^{83}Kr. Note that use of two different pumping lines from the $1s_5$ state is necessary due to selection rules and the weakness of the $F'=9/2-F''=9/2$ transition. Note also that all hfs are inverted.

IV. HYPERFINE SPECTRA

Examples of our two-step laser spectra used to measure hyperfine splittings in the $4p^55d$ configuration of ^{83}Kr are shown in Figs. 3 and 4. These spectra represent sub-Doppler absorption dips in the transmitted power of the laser beam that originates in laser 2 and passes through the target cell. Each peak corresponds to a specific hfs transition between an intermediate hfs level in the $4p^55p$ manifold and a selected final level in the $4p^55d$ manifold.

The spectrum on the left in Fig. 3 provides a measurement of the $F''=7/2$ to $F''=11/2$ splitting in the $4d_5$ state. To obtain this spectrum, ^{83}Kr atoms are first excited from the metastable $1s_5$ $F=11/2$ level to the $2p_{10}$ $F'=9/2$ intermediate level using 892.869-nm light from laser 1. Then laser 2, whose frequency scans linearly in time in the vicinity of 791.342 nm, promotes these atoms further into the $F''=7/2$ and $11/2$ levels of the $4d_5$ state. The predicted intensities of these transitions confirm the identities of the individual spectral features [12]. For instance, the predicted intensities of the aforementioned transitions from $F'=9/2$ to $F''=7/2$, $9/2$, and $11/2$ fall in the ratio of 1.0:0.04:1.0. The $F'=9/2-F''=9/2$ feature is undetectable in our spectrum because it is so weak. Using the comb of Fabry-Perot interference fringes, we evaluate the frequency separation between the two features, thereby determining an $F''=7/2-11/2$ splitting of 628.0(3) MHz for the $4d_5$ state.

The spectrum on the right side of Fig. 3 provides a measurement of the $F''=9/2-11/2$ splitting in the $4d_5$ state. Transitions to these two levels originate in the $1s_5$ $F=13/2$ state from which the ^{83}Kr are excited into the $2p_{10}$ $F'=11/2$ level. The predicted intensities for the $F'=11/2-F''=9/2$ and $11/2$ transitions are in the ratio 1.0: 0.7. The fact that the two peaks in our spectrum are essentially the same height suggests that the intensity of the beam from laser 2 varies slightly with the scanning of the laser. Once again, we use careful matching of the Fabry-Perot interferogram to the separation of the spectral peaks to arrive at a splitting of 403.3(2) MHz between the $F''=9/2$ and $11/2$ peaks.

As noted earlier, measurements of two splittings in a particular manifold are sufficient to evaluate hyperfine coupling constants for that manifold. However, our inability to obtain a pair of measurements from a single spectrum (due to intensities or selection rules) forces us in three of the four cases to use two separate spectra as shown in Fig. 3. To be specific, we employ this two-spectra approach to determine hyperfine splittings in the $4d_1'$ and $4d_4$ states as well as the $4d_5$ state.

In the case of the $4d_3$ state, only one spectrum is required as shown in Fig. 4. This spectrum provides the $F''=9/2-11/2$ and $F''=11/2-13/2$ splittings in the $4d_3$ state. A 760.154-nm laser promotes ^{83}Kr atoms from the $1s_5$ $F=13/2$ level into the $2p_6$ $F'=11/2$ level. These atoms are
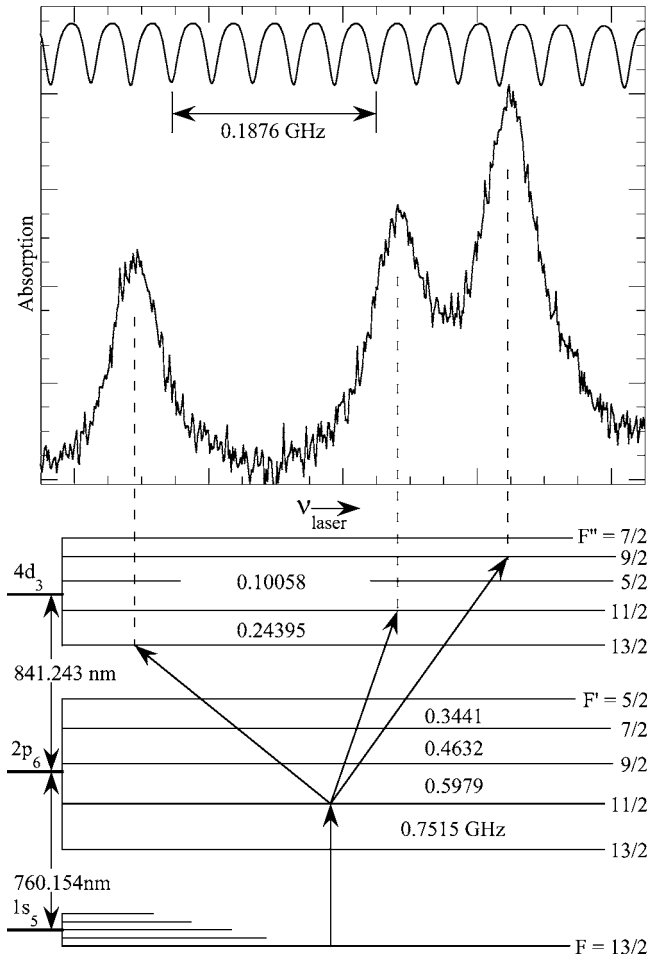
FIG. 4. Two-step spectra and excitation schemes for measuring hfs in $4d_3$ state of ^{83}Kr. Note that all hfs structures are inverted, and the order of the hfs levels is irregular in the $4d_3$ manifold.

then further promoted into the $4d_3$ $F''=9/2$, 11/2, and 13/2 levels by 841.243-nm laser light. These are the only allowed transitions into the $4d_3$ state from the $2p_6$ $F'=11/2$ level. The predicted transition intensities into the $F''=9/2$, 11/2, and 13/2 levels fall in the ratio 0.7: 0.85: 1.0 and therefore confirm our spectral identifications. We suppress extraneous peaks in our spectra by carefully fixing laser 1 on the desired first-step transition.

Consider the width of the spectral features. Under ideal conditions, Doppler broadening would be negligible due to the sweepless, narrow-band, velocity-selective nature of the first step of excitation. In the complete absence of Doppler broadening, the full width at half maximum linewidth of our absorption features would be $\Delta\omega = \gamma(1+F)$, where $F \equiv (1 +I/I_{sat})^{1/2}$ is a power broadening factor, and

$$\gamma = 1/\tau_1 + 1/\tau_2 + 2/T + 2/\tau_{coll} + \Delta\omega_{laser} \qquad (8)$$

is the homogenous linewidth in rad/sec. In this expression, τ_1 is the lifetime of the intermediate $2p_{10}$, $2p_8$, or $2p_6$ state and τ_2 is the lifetime of the $4p^5 5d$ state of interest. Since the $2p_i$ lifetimes are about 30 nsec and the lifetimes of our final states exceed 100 nsec, an unbroadened Doppler-free natural

linewidth would be about 40 Mrad/sec or 7 MHz. Transit time and collisional broadening $2/T$ and $2/\tau_{coll}$ along with laser linewidth broadening $\Delta\omega_{laser}$ (each of which is about 6 Mrad/sec or 1 MHz) would then bring the total γ to about 10 MHz, which is still much smaller than our experimentally observed widths of 60 MHz. These experimental widths of 60 MHz cannot stem from power broadening since our experimental beam intensities $I \approx 2$ mW/mm^2 are far less than the estimated saturation intensities $I_{sat} \approx 100$ mW/mm^2 for the second step of excitation. It therefore appears that the observed 60-MHz widths reflect a modest amount of Doppler broadening that creeps back into the second step of excitation by way of velocity-changing collisions. Such collisions introduce a small spread in the velocities of the ^{83}Kr atoms that occupy the intermediate $2p_{10}$, $2p_8$, or $2p_6$ states; the range of these velocities corresponds to about ± 25 MHz of Doppler detuning. Broadening of this sort due to velocity-changing collisions between excited and ground-state krypton atoms has been investigated at considerable depth [13].

Besides exploring the $4d_1'$, $4d_3$, $4d_4$, $4d_5$, and $4d_6$ (since $J=0$ for the $4d_6$ state, it has no hfs) states, we aim to measure the hfs in the $4d_1''$ and $4d_2$ states using 769.454/788.176 nm or 810.436/777.628 nm to observe the $4d_1''$ state, and 769.454/788.176 nm to observe the $4d_2$ state. In our attempts thus far, small S/N ratios have thwarted the extraction of meaningful hyperfine splittings from the spectra. We expect to rectify this situation in the near future through changes in the target cell and increased laser intensities.

V. RESULTS AND DISCUSSION

Using averaged frequency splittings derived from 20 or more spectra resembling those in Figs. 3 and 4, we have evaluated hyperfine coupling constants for four different fine-structure states in the $4p^5 5d$ configuration. These averaged coupling constants and hyperfine separations are collected in Table I, where the quoted uncertainties are primarily statistical and represent one standard error (one standard deviation of the mean). The first property to note in these results is that all values of A are negative, thereby indicating that all four hyperfine structures are inverted as in the case of the $4p^5 5s$ and $4p^5 5p$ manifolds. Inverted hfs is fairly common in heavier atoms where relativistic, electron-correlation, core-polarization, and configuration-mixing contributions to fine and hyperfine structures can be significant. A second point to notice here is that the values of A vary considerably from one $4d_i$ state to another, which implies that the effective magnetic field B_{el} at the nucleus varies widely among the four $4d_i$ states that we have examined.

The electric quadrupole coupling constant, B, also varies considerably indicating that the electric-field gradient at the nucleus varies significantly among these $4p^5 5d$ states. For the $4d_1'$ state, B even changes sign indicating that the electric-field gradient reverses direction as compared to the other three cases.

The larger the value of B compared to that of A, the larger the deviation of the hfs from the interval rule [Eq. (4)]. The ratio B/A ranges from 0.89 for the $4d_5$ state to 12.6 for the

TABLE I. Hyperfine-coupling constants A and B (in MHz) for four different $4p^55p$ states of ^{83}Kr. The experimentally determined values of the hyperfine splittings used in the evaluation of the A's and B's are included. The coupling constants evaluated by Cannon for $4d_4'$ are also included [2].

State	A	B	$7/2-11/2$	$9/2-11/2$	$11/2-13/2$	$13/2-15/2$
$4d_1'$	−60.6(2)	+85(4)			385(1)	419.2(8)
$4d_3$	−18.29(5)	−231(1)		100.6(3)	244.0(4)	
$4d_4$	−104.31(15)	−409(3)		536(1)		952.8(2)
$4d_5$	−63.97(6)	−56.2(7)	628.0(3)	403.3(2)		
$4d_4'$[a]	−73.66(2)	−455.0(8)				

[a]Reference [2].

$4d_3$ state indicating that of all four $4d_i$ states examined, the structure of the $4d_5$ state comes closest to satisfying the interval rule and the $4d_3$ structure departs the most. This departure of the $4d_3$ structure is so severe that even the ordering of the hfs levels is scrambled as shown in Fig. 4.

We conclude that any further inferences drawn from the signs and values of these coupling constants must await a theoretical analysis that takes relativistic effects, electron-correlation, core-polarization, and/or configuration mixing into account.

[1] E. Rasmussen and V. Middleboe, K. Dan. Vidensk. Selsk. Mat. Fys. Medd. **30**, No. (3) (1955), and earlier references cited therein; D. A. Jackson, J. Opt. Soc. Am. **67**, 1638 (1977); R. J. Champeau and J. C. Keller, J. Phys. B **11**, 391 (1978); X. Husson, J. P. Grandin, and H. Kucal, J. Phys. B **12**, 3883 (1979); H. Gerhardt *et al.*, Hyperfine Interact. **9**, 175 (1981); H. Abu Safia and X. Husson, J. Phys. (Paris) **45**, 863 (1984); K. Heilig and A. Steudel, *Physics of Atoms and Molecules A*, edited by W. Hanle and H. Kleinpoppen (Plenum, New York, 1978), p. 263; J. R. Brandenberger, Phys. Rev. A **39**, 64 (1989); T. Trickl, M. J. J. Vrakking, E. Cromwell, Y. T. Lee, and A. H. Kung, *ibid.* **39**, 2948 (1989); B. D. Cannon and G. R. Janik, *ibid.* **42**, 397 (1990); S. C. Parker and J. R. Brandenberger, *ibid.* **44**, 3354 (1991).

[2] B. D. Cannon, Phys. Rev. A **47**, 1148 (1993).

[3] J. R. Brandenberger, C. A. Regal, R. O. Jung, and M. C. Yakes, Phys. Rev. A **65**, 042510–1 (2002).

[4] The isotopically enriched krypton gas was supplied by Isotec, Inc.

[5] The 30-MHz oscillator used here is a variant on the design discussed in W. E. Bell, A. L. Bloom, and J. Lynch, Rev. Sci. Instrum. **32**, 688 (1961).

[6] J. R. Brandenberger, Phys. Rev. A **36**, 76 (1987).

[7] All wavelengths quoted in this paper are measured in air.

[8] By a $v \approx 0$ velocity group, we mean ^{83}Kr atoms whose velocity components parallel to the laser beams are essentially zero.

[9] The scanning of an external cavity diode laser can exhibit small nonuniformities or nonlinearities due to (i) competition between the resonances of the laser's internal and external cavities and (ii) nonlinearity in the expansion of the piezoelectric crystal that tunes the external cavity.

[10] These commercially available diode lasers are manufactured or distributed by Sharp, Sanyo, Toptica, Roithner, Thorlabs, and Optima Precision.

[11] Lloyd Armstrong, Jr., *Theory of the Hyperfine Structure of Free Atoms* (Wiley-Interscience, New York, 1971).

[12] The expressions that predict the intensities of these lines first appeared in H. E. White and A. Y. Eliason, Phys. Rev. **44**, 753 (1933).

[13] C. Bréchignac and R. Vetter, Phys. Rev. A **22**, 496 (1979).